Mycobacterium tuberculosis is protected from NADPH oxidase and LC3-associated phagocytosis by the LCP protein CpsA

Stefan Köster[a,1], Sandeep Upadhyay[b,c,1], Pallavi Chandra[b,c], Kadamba Papavinasasundaram[d], Guozhe Yang[b,c], Amir Hassan[b,c], Steven J. Grigsby[b,c], Ekansh Mittal[b,c], Heidi S. Park[a], Victoria Jones[e], Fong-Fu Hsu[f], Mary Jackson[e], Christopher M. Sassetti[d], and Jennifer A. Philips[b,c,2]

[a]Division of Infectious Diseases, Department of Medicine, New York University School of Medicine, New York, NY 10016; [b]Division of Infectious Diseases, Department of Medicine, Washington University School of Medicine, St. Louis, MO 63110; [c]Department of Molecular Microbiology, Washington University School of Medicine, St. Louis, MO 63110; [d]Department of Microbiology and Physiological Systems, University of Massachusetts Medical School, Worcester, MA 01655; [e]Mycobacteria Research Laboratories, Department of Microbiology, Immunology and Pathology, Colorado State University, Fort Collins, CO 80523; and [f]Mass Spectrometry Resource, Division of Endocrinology, Diabetes, Metabolism, and Lipid Research, Department of Medicine, Washington University School of Medicine, St. Louis, MO 63110

Edited by Lalita Ramakrishnan, University of Cambridge, Cambridge, United Kingdom, and approved September 5, 2017 (received for review May 10, 2017)

***Mycobacterium tuberculosis*' success as a pathogen comes from its ability to evade degradation by macrophages. Normally macrophages clear microorganisms that activate pathogen-recognition receptors (PRRs) through a lysosomal-trafficking pathway called "LC3-associated phagocytosis" (LAP). Although *M. tuberculosis* activates numerous PRRs, for reasons that are poorly understood LAP does not substantially contribute to *M. tuberculosis* control. LAP depends upon reactive oxygen species (ROS) generated by NADPH oxidase, but *M. tuberculosis* fails to generate a robust oxidative response. Here, we show that CpsA, a LytR-CpsA-Psr (LCP) domain-containing protein, is required for *M. tuberculosis* to evade killing by NADPH oxidase and LAP. Unlike phagosomes containing wild-type bacilli, phagosomes containing the Δ*cpsA* mutant recruited NADPH oxidase, produced ROS, associated with LC3, and matured into antibacterial lysosomes. Moreover, CpsA was sufficient to impair NADPH oxidase recruitment to fungal particles that are normally cleared by LAP. Intracellular survival of the Δ*cpsA* mutant was largely restored in macrophages missing LAP components (*Nox2*, *Rubicon*, *Beclin*, *Atg5*, *Atg7*, or *Atg16L1*) but not in macrophages defective in a related, canonical autophagy pathway (*Atg14*, *Ulk1*, or *cGAS*). The Δ*cpsA* mutant was highly impaired in vivo, and its growth was partially restored in mice deficient in NADPH oxidase, *Atg5*, or *Atg7*, demonstrating that CpsA makes a significant contribution to the resistance of *M. tuberculosis* to NADPH oxidase and LC3 trafficking in vivo. Overall, our findings reveal an essential role of CpsA in innate immune evasion and suggest that LCP proteins have functions beyond their previously known role in cell-wall metabolism.**

M. tuberculosis | autophagy | LC3-associated phagocytosis | NADPH oxidase | LytR-CpsA-Psr

The pathogen *Mycobacterium tuberculosis* (Mtb) causes one of the world's deadliest infections. Mtb survives within macrophages by preventing its own delivery to the degradative, phagolysosomal compartment (1). Recent work distinguished two related phagolysosomal pathways that are characterized by the association of LC3 with the phagosomal membrane, macroautophagy (hereafter autophagy) and LC3-associated phagocytosis (LAP) (2–5). Autophagy involves the capture of cytoplasmic components by a double-membrane compartment called the "autophagosome." When this process sequesters microorganisms, it is called "xenophagy." In both xenophagy and LAP, LC3-decorated organelles fuse with lysosomes, resulting in bacterial degradation. However, neither pathway is effective against Mtb. Only a small fraction of Mtb colocalizes with LC3, and autophagy-related (Atg) proteins that are required for both LAP and xenophagy make only a modest contribution toward Mtb control (6–13), suggesting that Mtb is able to circumvent both processes. A number of host and bacterial factors contribute to Mtb's ability to evade autophagy (14–17). How Mtb inhibits LAP is unclear.

LAP is initiated by bacterial binding to pathogen-recognition receptors (PRRs) (Fig. S1). LAP requires NADPH oxidase and the class III phosphatidylinositol 3-kinase complex, which generate reactive oxygen species (ROS) and phosphatidylinositol 3-phosphate [PI(3)P], respectively, at the incipient phagosome (2, 3, 5). ROS directly kill bacteria and, along with PI(3)P, recruit the Atg conjugation systems that deposit LC3 on the phagosomal membrane. Mtb activates numerous PRRs, so it is surprising that Mtb does not robustly trigger LAP. This incongruity suggests that Mtb has a LAP evasion strategy.

Here, we show that an exported Mtb protein, CpsA (Rv3484), prevents clearance of Mtb by NADPH oxidase and LAP. CpsA contains two domains: a LytR-CpsA-Psr (LCP) domain, which is found widely in Gram-positive bacteria, and a LytR domain, which has an unknown function. LCP domains can transfer cell-wall teichoic acids from their lipid-bound precursors to peptidoglycan (PGN) (18–20). Although mycobacteria do not have teichoic acid, arabinogalactan (AG) is linked to PGN in an analogous manner. Mtb has three proteins with LCP and LytR domains: Rv3267/Lcp1/CpsA1, Rv3484/CpsA/CpsA2, and Rv0822c.

Significance

***Mycobacterium tuberculosis* (Mtb), the causative agent of the disease tuberculosis, grows in macrophages, cells that normally kill bacteria. Recent work has defined a macrophage pathway called "LC3-associated phagocytosis" (LAP) that can eliminate other microbes. LAP is characterized by the recruitment of NADPH oxidase to phagosomes, followed by phagosomal association with LC3 and delivery of the bacteria to a degradative lysosome. Here, we show that LAP does not effectively clear Mtb. The ability of Mtb to inhibit LAP and therefore cause disease depends upon CpsA, a member of the LytR-CpsA-Psr (LCP) protein family, which has previously been implicated in cell-wall metabolism. We demonstrate that Mtb CpsA plays an unexpected role in antagonizing host innate immunity by inhibiting NADPH oxidase and LAP.**

Author contributions: S.K., S.U., P.C., and J.A.P. designed research; S.K., S.U., P.C., A.H., S.J.G., E.M., H.S.P., V.J., and F.-F.H. performed research; S.K., S.U., P.C., K.P., G.Y., S.J.G., M.J., and C.M.S. contributed new reagents/analytic tools; S.K., S.U., P.C., A.H., E.M., M.J., and J.A.P. analyzed data; and S.K. and J.A.P. wrote the paper.

The authors declare no conflict of interest.

This article is a PNAS Direct Submission.

[1]S.K. and S.U. contributed equally to this work.

[2]To whom correspondence should be addressed. Email: philips.j.a@wustl.edu.

This article contains supporting information online at www.pnas.org/lookup/suppl/doi:10.1073/pnas.1707792114/-/DCSupplemental.

Rv3267 is highly conserved in mycobacteria and is the main ligase responsible for catalyzing the transfer of AG to PGN (21, 22). CpsA shares 36% sequence identity with Rv3267; however, unlike Rv3267, CpsA is not conserved in rapidly growing, nonpathogenic mycobacteria (23), and the Δ*cpsA* mutant does not exhibit significant cell-wall defects (21). Here, we demonstrate that Mtb CpsA plays an unexpected role in antagonizing host innate immunity by inhibiting NADPH oxidase and LAP. Our findings provide an explanation for the limited oxidative burst seen in response to Mtb and establish a role for CpsA in inhibiting innate immune clearance of Mtb.

Results

CpsA Protects Mtb from Lysosomal Clearance. Previously, we screened secreted Mtb proteins for interactions with human proteins using a high-throughput yeast two-hybrid assay (24). CpsA was included in this screen because it had a predicted signal peptide, and it had been found in culture filtrate in mass spectrometry studies (25–27). We found that CpsA interacts with T-cell leukemia virus type I binding protein 1 (TAX1BP1) and nuclear dot protein 52 kDa (NDP52), two paralogs involved in xenophagy (13, 28, 29). This prompted us to delete *cpsA* from the WT H37Rv strain of Mtb to characterize its effect on autophagy (Fig. S2). When we infected LC3-GFP–expressing murine bone marrow-derived macrophages (BMDMs), we found that the Δ*cpsA* mutant was three times more likely to be in an LC3-GFP$^+$ compartment than the WT strain at 4 h postinfection (hpi) (Fig. 1 *A* and *B*). We quantified the mean fluorescence intensity (MFI) around individual phagosomes using automated image analysis, as previously described in detail (24). We found a significant shift in Δ*cpsA* mutant phagosomes to brighter GFP populations compared with WT Mtb phagosomes (Fig. 1*C*), which closely approximated our visual scoring. The enhanced colocalization of the mutant with LC3-GFP was restored to WT levels in the complemented strain (Δ*cpsA*::*cpsA*) (Fig. 1*C*). As shown previously, activating macrophages with IFN-γ before infection enhanced LC3 association with WT Mtb (Fig. 1*D*) (7, 11, 30, 31). In contrast to the marked enhancement of LC3 association with the Δ*cpsA* mutant in unactivated macrophages, there was little difference between WT and Δ*cpsA* in IFN-γ–activated macrophages (Fig. 1*D*). Thus, CpsA inhibited LC3-associated trafficking specifically in unactivated macrophages.

To determine whether enhanced LC3 trafficking resulted in increased lysosomal delivery, we quantified the colocalization of the Δ*cpsA* mutant with lysosomal-associated membrane protein 1 (LAMP1), a late endosomal and lysosomal marker. We found that LAMP1 colocalized with the Δ*cpsA* mutant significantly more than it did with WT Mtb at 4 hpi, similar to what was seen when macrophages were pretreated with IFN-γ, which promotes lysosomal trafficking (Fig. 1 *E*–*G*). LAMP1 colocalization was restored to WT levels in the complemented strain (Fig. 1*F*). There was no increased association of LAMP1 with the Δ*cpsA* mutant relative to WT Mtb in IFN-γ–activated macrophages, again suggesting that the altered trafficking was predominantly seen in unactivated macrophages (Fig. 1*G*). To determine whether the increased phagolysosomal trafficking depended upon autophagy proteins, we examined LAMP1 colocalization with Mtb in macrophages genetically lacking *Atg5*, which is required for both xenophagy and LAP (Fig. S1). In such macrophages, the enhanced association of LAMP1 with the Δ*cpsA* mutant was abrogated (Fig. 1*H*).

Next, we examined whether the failure of the Δ*cpsA* mutant to arrest lysosomal trafficking impaired its intracellular survival. We found that the Δ*cpsA* mutant, which grew normally in liquid medium (Fig. S3*A*), was killed by murine BMDMs, whereas WT Mtb and the complemented strain survived (Fig. 2*A*). IFN-γ–naive BMDMs cleared the Δ*cpsA* mutant to a similar degree as IFN-γ–activated macrophages controlled WT Mtb. We had similar findings in human THP-1 macrophages (Fig. 2*B*). To evaluate whether Δ*cpsA* was killed as a consequence of lysosomal trafficking, we used previously validated siRNA pools to deplete Ras-related protein Rab-7a (RAB7) or tumor-susceptibility gene 101 (TSG101), which are required for phagosome maturation (Fig. S4) (24, 32, 33). Silencing *Rab7* or *Tsg101* before infection partially restored the intracellular survival of Δ*cpsA* (Fig. 2 *C* and *D* and Fig. S4). Combined, these results suggested that CpsA protects Mtb from killing by an LC3-associated lysosomal-trafficking pathway.

CpsA Protects Mtb from LAP. Both xenophagy and LAP depend upon a common set of factors to deliver LC3 to the phagosomal membrane, including BECLIN1, ATG7, ATG5, and ATG16L1 (Fig. S1). To determine whether these shared factors were important in clearing the Δ*cpsA* mutant, we examined macrophages in which we silenced *Atg7* or that were genetically lacking *Atg5*, *Atg16L1*, or *Beclin1* for their ability to kill the Δ*cpsA* mutant. In all cases, macrophages defective in these core autophagy proteins were impaired in clearing the Δ*cpsA* mutant relative to WT macrophages (Fig. 3 *A*–*D* and Fig. S4). These results are consistent with the idea that CpsA protects Mtb from killing by an LC3-associated lysosomal-trafficking pathway, but they do not distinguish whether that pathway is LAP or xenophagy. Recent studies have defined distinct genetic requirements for xenophagy and LAP (4). Xenophagy requires the autophagy initiation machinery (ULK1, ATG14, and others), which is dispensable for LAP, whereas LAP requires the NADPH oxidase and RUBICON (Fig. S1). When we examined *Ulk1*-silenced and *Atg14*-deficient macrophages, we observed a large discrepancy between WT Mtb and Δ*cpsA* survival (Fig. 3 *E* and *F* and Fig. S4). In addition, Mtb xenophagy depends upon the cGMP-AMP synthetase (*cGAS*) (12, 34–36). As we found with macrophages defective in the xenophagy-specific components ULK1 and ATG14, the intracellular growth defect of the Δ*cpsA* mutant was not rescued in macrophages lacking *cGAS* (*Cgas*$^{-/-}$) (Fig. 3*G*). In addition, whereas *Atg5* deficiency reversed the enhanced association of LAMP1 with the Δ*cpsA* mutant, the absence of *Cgas* did not (Figs. 1*H* and 3*H*). Moreover, when we examined the transcriptional response of macrophages infected with WT or Δ*cpsA*, there was no difference in the magnitude of the transcriptional response activated by cGAS (called the "cytosolic-surveillance pathway") (Fig. S5). These data suggested that xenophagy and the cGAS-dependent pathway previously characterized during Mtb infection were not responsible for clearing the Δ*cpsA* mutant.

One distinction between xenophagy and LAP is the role of RUBICON, which inhibits autophagy and is required for LAP (4, 37, 38). In macrophages in which *Rubicon* was genetically absent or silenced, the attenuation of Δ*cpsA* was nearly completely rescued (Fig. 3 *I* and *J* and Fig. S4), consistent with the idea that Δ*cpsA* is cleared by LAP. Examining all our data together revealed that the Δ*cpsA* mutant was restored to ∼80% of WT levels in macrophages selectively impaired in LAP (*Rubicon*) or jointly defective in xenophagy and LAP (*Beclin*, *Atg5*, *Atg7*, or *Atg16L1*) (Fig. 3*K*). In contrast, there was little rescue of the survival of the Δ*cpsA* mutant in macrophages defective only in xenophagy (*Atg14*, *Ulk1*, and *cGAS*) (Fig. 3*K* and Fig. S1). We conclude that LAP, not xenophagy, plays the predominant role in clearing the Δ*cpsA* mutant.

CpsA Acts Upstream of NADPH Oxidase. In addition to a requirement for RUBICON, LAP also depends upon NADPH oxidase and ROS (4, 5), which are not required for xenophagy. To see if NADPH oxidase also played a role in clearing the Δ*cpsA* mutant, we examined its survival in *Nox2*-KO macrophages, which lack the NADPH oxidase catalytic core (gp91^{phox}). We compared Δ*cpsA* to a mutant lacking *katG*, which encodes a catalase-peroxidase. As previously described, the Δ*katG* mutant was attenuated in WT macrophages and survived in *Nox2*-KO macrophages (Fig. 4*A*) (39). The Δ*cpsA* mutant behaved similarly; it was attenuated in WT BMDMs, and its intracellular survival was restored in *Nox2*-KO macrophages (Figs. 3*K* and 4*A*), consistent with its being cleared by LAP. In contrast, there was no rescue of Δ*cpsA* in BMDMs lacking inducible nitric oxide synthase (*NOS2*$^{-/-}$) (Fig. 3*K*). However, while both Δ*katG* and Δ*cpsA* were similarly susceptible to NADPH oxidase inside macrophages, the Δ*cpsA* mutant was not nearly as susceptible to ROS in liquid medium

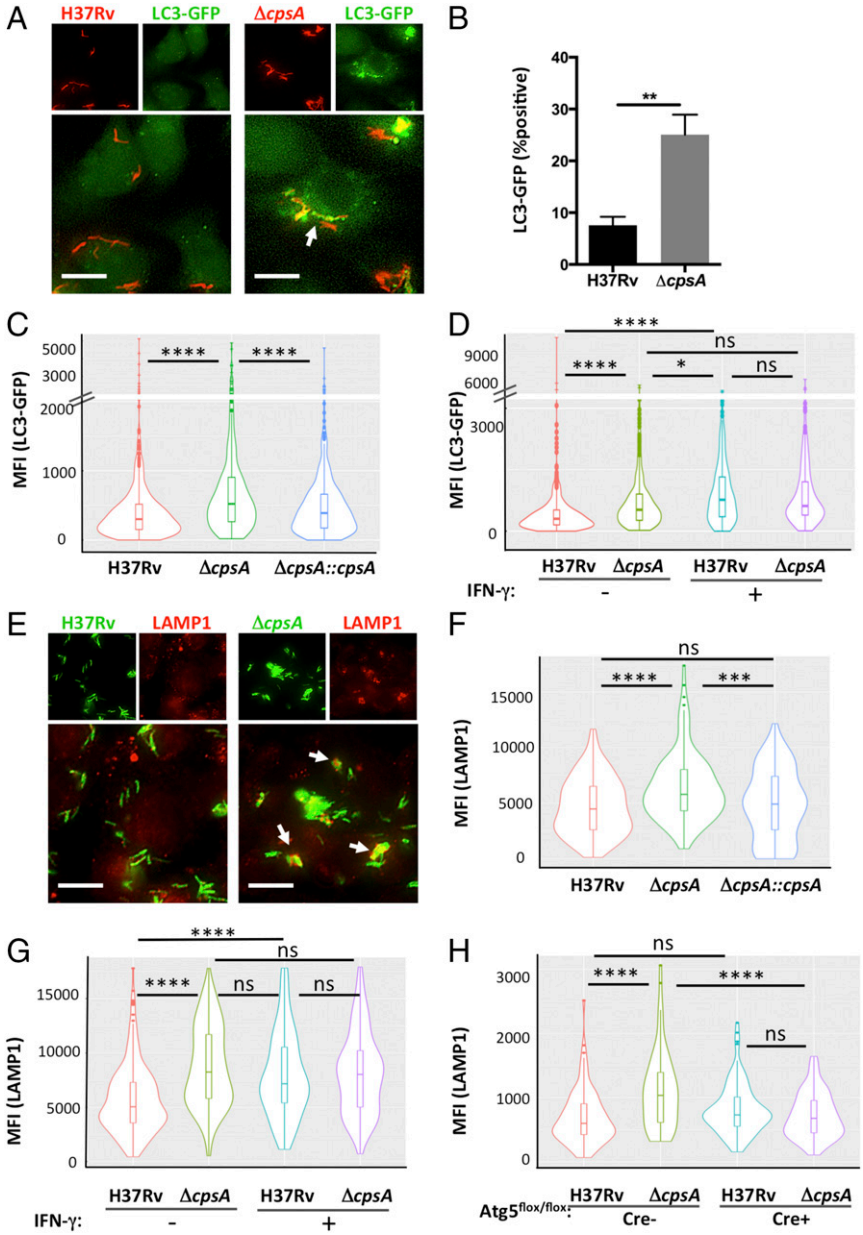

Fig. 1. CpsA inhibits LC3-associated lysosomal trafficking. (*A*) Fluorescence imaging of DsRed-expressing H37Rv or Δ*cpsA* (red) 4 hpi in murine BMDMs expressing GFP-LC3 (green). (*B*) The percentage of bacteria in an LC3-GFP$^+$ phagosome at 4 hpi was quantified by a blinded observer from over 500 bacteria in two independent experiments. $^{**}P = 0.0017$, Student's *t* test. (*C*) Automated image analysis was used to quantify the GFP MFI colocalized with over 250 bacilli, as shown in violin plots (described below). (*D*) Phagosomal LC3-GFP was quantified 4 hpi from BMDMs pretreated with IFN-γ or vehicle control before infection. (*E*) Immunofluorescence (IF) microscopy of LAMP1- (red) and GFP-expressing H37Rv or Δ*cpsA* (green) 4 hpi in BMDMs. (*F* and *G*) Phagosomal LAMP1 MFI in BMDMs pretreated with IFN-γ or vehicle control before infection was quantified at 4 hpi (*F*) and 24 hpi (*G*) from at least 100 bacilli. (*H*) Phagosomal LAMP1 MFI was quantified 4 hpi from *Atg5*-KO BMDMs (*Atg5*$^{flox/flox}$ LysM-Cre$^+$) and controls (*Atg5*$^{flox/flox}$ LysM-Cre$^-$) from at least 70 bacilli per sample. In *A* and *E*, arrows indicate bacilli that colocalize with the cellular marker. (Scale bars, 10 μm.) In *C*, *D*, and *F*–*H*, no contrast adjustment was performed before automated image analysis. The violin plots show the distribution of the data (the MFI of the indicated cellular marker associated with distinct intracellular bacteria) as its probability density. Within the violin plot, the box and whiskers plot indicates the median (horizontal line) and interquartile range (IQR) (boxes). The upper whisker extends to 1.5 × IQR from the top of the top box, and the lower whisker extends from the lower box by 1.5 × IQR IQR. Any data beyond the end of the whiskers are outlying points that are plotted individually. Data show one representative experiment from at least two independent experiments. $^*P \leq 0.05$; $^{***}P \leq 0.0005$; $^{****}P \leq 0.0001$; ns, not significant; one-way ANOVA with Tukey's multiple comparisons test.

(Fig. S3*B*). Thus, we considered the possibility that Δ*cpsA* might be susceptible to NADPH oxidase because it induced more ROS during infection. To visualize ROS, we used 2′,7′-dichlorodihydrofluorescein diacetate (H_2DCFDA), a cell-permeant derivative of fluorescein that fluoresces upon oxidation. We found that Δ*cpsA* infection generated substantially more phagosomal ROS than WT Mtb in both murine BMDMs and human THP-1 cells (Fig. 4 *B*–*D*). The observed H_2DCFDA fluorescence was dependent upon ROS, as it could be blocked by diphenyleneiodonium (DPI), an inhibitor of superoxide production. Moreover, the ROS generated by Δ*cpsA* was attributable to NADPH oxidase, as it was largely absent in *Nox2*-KO macrophages (Fig. 4*C*). It has been shown previously that NADPH oxidase lies upstream of the Atg conjugation systems in LAP (Fig. S1) (4, 40). Consistent with

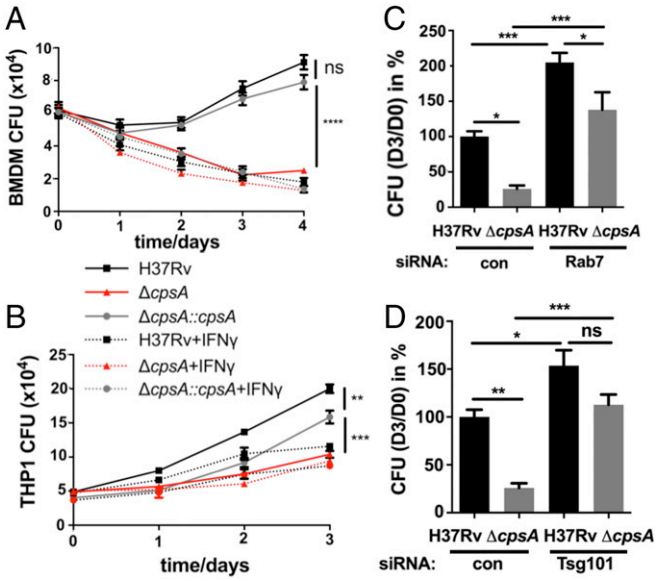

Fig. 2. Mtb require CpsA to survive in macrophages. (*A* and *B*) Survival of H37Rv, Δ*cpsA*, and Δ*cpsA::cpsA* in BMDMs (*A*) and human THP-1 cells (*B*) that were pretreated with either IFN-γ or vehicle. Data show the mean ± SEM of one representative experiment from at least two independent experiments. In some cases the error bar is shorter than the height of the symbol. $^{**}P \leq 0.01$, $^{***}P \leq 0.001$, $^{****}P \leq 0.0001$, ns, not significant, one-way ANOVA with Tukey's multiple comparisons test of H37Rv, Δ*cpsA*, and Δ*cpsA::cpsA* at the last time point. (*C* and *D*) Survival of H37Rv and Δ*cpsA* in BMDMs treated with siRNA control (con) or siRNA-targeting Rab7 (*C*) or Tsg101 (*D*) for 2 d before infection. The ratios of cfu 3 d after infection relative to day 0 were normalized to the H37Rv control samples. Data show the mean + SEM from one representative experiment with at least three replicates from at least two independent experiments; $^{*}P \leq 0.05$; $^{**}P \leq 0.01$; $^{***}P \leq 0.0005$; ns, not significant; one-way ANOVA with Tukey's multiple comparisons test.

those findings, *Atg5* was not required for the enhanced phagosomal ROS generated by the Δ*cpsA* mutant (Fig. 4*E*). Since the Δ*cpsA* mutant can grow in macrophages lacking *Atg5* (Fig. 3*B*) even though there is enhanced ROS (Fig. 4*E*), it suggests that Δ*cpsA* is not killed by ROS alone; clearance also depends upon the Atg conjugation system and lysosomal trafficking. Combined, these data demonstrate that CpsA protects Mtb from NADPH oxidase and subsequent LAP-mediated killing.

CpsA Blocks NADPH Oxidase Recruitment to Mtb Phagosomes. NADPH oxidase is composed of two integral membrane subunits ($p22^{phox}$ and $gp91^{phox}$) that form flavocytochrome b_{558} and a trimeric cytosolic complex ($p40^{phox}$, $p47^{phox}$, and $p67^{phox}$). NADPH oxidase activity requires membrane trafficking of flavocytochrome b_{558} from recycling endosomes (41), assembly with the cytosolic subunits, and activation, which is contingent upon recruitment of GTP-bound Rac1/2 (42). Since the Δ*cpsA* mutant elicited more ROS, we assessed NADPH oxidase trafficking and assembly by examining recruitment of $gp91^{phox}$, $p40^{phox}$, and $p47^{phox}$ to mycobacterial phagosomes. We found that the Δ*cpsA* mutant colocalized with the membrane and cytosolic components of NADPH oxidase substantially more than WT Mtb (Fig. 5 *A*–*G*). As expected, the enhanced association was abrogated in *Nox2*-KO BMDMs (Fig. 5 *C*, *E*, and *G*). In contrast, enhanced colocalization of the NADPH oxidase with the Δ*cpsA* mutant did not depend upon *Atg5* (Fig. 5 *H*–*J*), corroborating that ROS generation did not depend upon the Atg conjugation system (Fig. 4*E*). These findings demonstrate that CpsA blocks NADPH oxidase recruitment to the mycobacterial phagosome.

CpsA Is Sufficient to Inhibit Phagosomal NADPH Oxidase Recruitment. CpsA belongs to the LCP family of proteins that are implicated in cell-wall biosynthesis in Gram-positive bacteria. Recent work demonstrated that in *Actinobacteria* LCP family members ligate AG to PGN (21, 22). In Mtb, there are two other full-length LCP members in addition to CpsA. Rv3267 plays the dominant role in cell-wall biogenesis, while CpsA is thought to have a minor role. Using GC/MS, we verified a slight decrease in AG attachment to PGN in the Δ*cpsA* mutant in our strain background, as had been seen in the CDC1551 strain background (Table S1). However, this did not result in substantial differences in growth under a variety of stress conditions (Fig. S3 *B*–*F*), as also is consistent with previous findings in the CDC1551 strain background (21).

Although the Δ*cpsA* mutant appeared to have only a mild cell-wall defect, we considered the possibility that even a mild perturbation in the cell wall might expose more pathogen-associated molecular patterns (PAMPs), rendering the Δ*cpsA* mutant hyperinflammatory and driving LAP. Since a number of Mtb Toll-like receptor 2 (TLR2) ligands are exported lipoproteins, we examined whether there was a difference in the proteins shed by the Δ*cpsA* mutant in culture filtrate compared with WT and the complemented strain. Mass spectrometry-based label-free quantitative analysis of the culture filtrate revealed no statistically significant differences except CpsA itself (Fig. S6). Since activation by other PAMPs was also possible, we next compared the transcriptional signature of uninfected macrophages with those infected with the Δ*cpsA* mutant and WT Mtb. At 4 hpi, thousands of genes were differentially regulated between uninfected and infected macrophages. However, using a false-discovery rate (FDR) cutoff of 0.05, only one gene was differentially expressed between WT and Δ*cpsA*–infected macrophages (TMA16, adjusted $P = 0.04$). Nonetheless, Kyto Encyclopedia of Genes and Genomes (KEGG) pathway analysis revealed a difference in the "Tuberculosis" response pathway between WT and Δ*cpsA*–infected macrophages, which largely reflected a difference in expression of NF-κB–regulated genes (Fig. S5*B*). However, contrary to our idea that the Δ*cpsA* mutant might drive LAP by virtue of being hyperinflammatory, the Δ*cpsA* mutant elicited a diminished NF-κB response (Fig. S5 *B*–*D*).

Since enhanced PAMP signaling from an altered cell wall did not appear to explain Δ*cpsA*'s ability to increase LAP, we wondered whether CpsA's role in virulence reflected a function independent of its activity on the cell wall. To determine whether CpsA was sufficient to alter intracellular trafficking in macrophages, we expressed a CpsA-GFP fusion protein in RAW264.7 cells, a murine macrophage cell line. CpsA has a putative signal peptide and is found in the culture filtrate as well as the cell envelope (Fig. S2) (25–27). We expressed CpsA without its putative signal peptide to mimic what would be exported from the bacteria and could gain access to the mammalian cell. As a control, we expressed a chloramphenicol acetyltransferase-fusion protein (CAT-GFP). We incubated macrophages expressing CpsA-GFP or CAT-GFP with zymosan, which has previously been shown to recruit the NADPH oxidase and traffic through the LAP pathway (4). We found that CpsA dramatically impaired recruitment of $p47^{phox}$ and $p40^{phox}$ to zymosan-containing phagosomes as well as their delivery to a $LAMP1^{+}$ compartment (Fig. 6 *A*–*F*). Thus, CpsA is sufficient to inhibit recruitment of NADPH oxidase to fungal cargo and to block lysosomal trafficking, demonstrating an activity beyond cell-wall biogenesis. Moreover, when the transfected macrophages were infected with the Δ*cpsA* mutant, CpsA expression inhibited recruitment of NADPH oxidase to Δ*cpsA*-mutant phagosomes and partially rescued the intracellular survival defect of the mutant, while WT Mtb infection was not altered (Fig. 6 *G* and *H*). Combined, these data support the idea that CpsA functions by acting on the host cell rather than the mycobacterial envelop to alter intracellular trafficking.

CpsA Protects Mtb in Vivo. To assess whether *cpsA* is required in vivo, we infected C57BL/6 mice with WT or Δ*cpsA* via low-dose aerosol. After 17 d of infection, there was more than a two-log reduction in cfu of Δ*cpsA* compared with WT Mtb in the lungs, along with diminished consolidation in the lungs and defective dissemination to the spleen (Fig. 7 *A*–*C*). Virulence was restored to the Δ*cpsA* mutant by introduction of *cpsA* under control of its

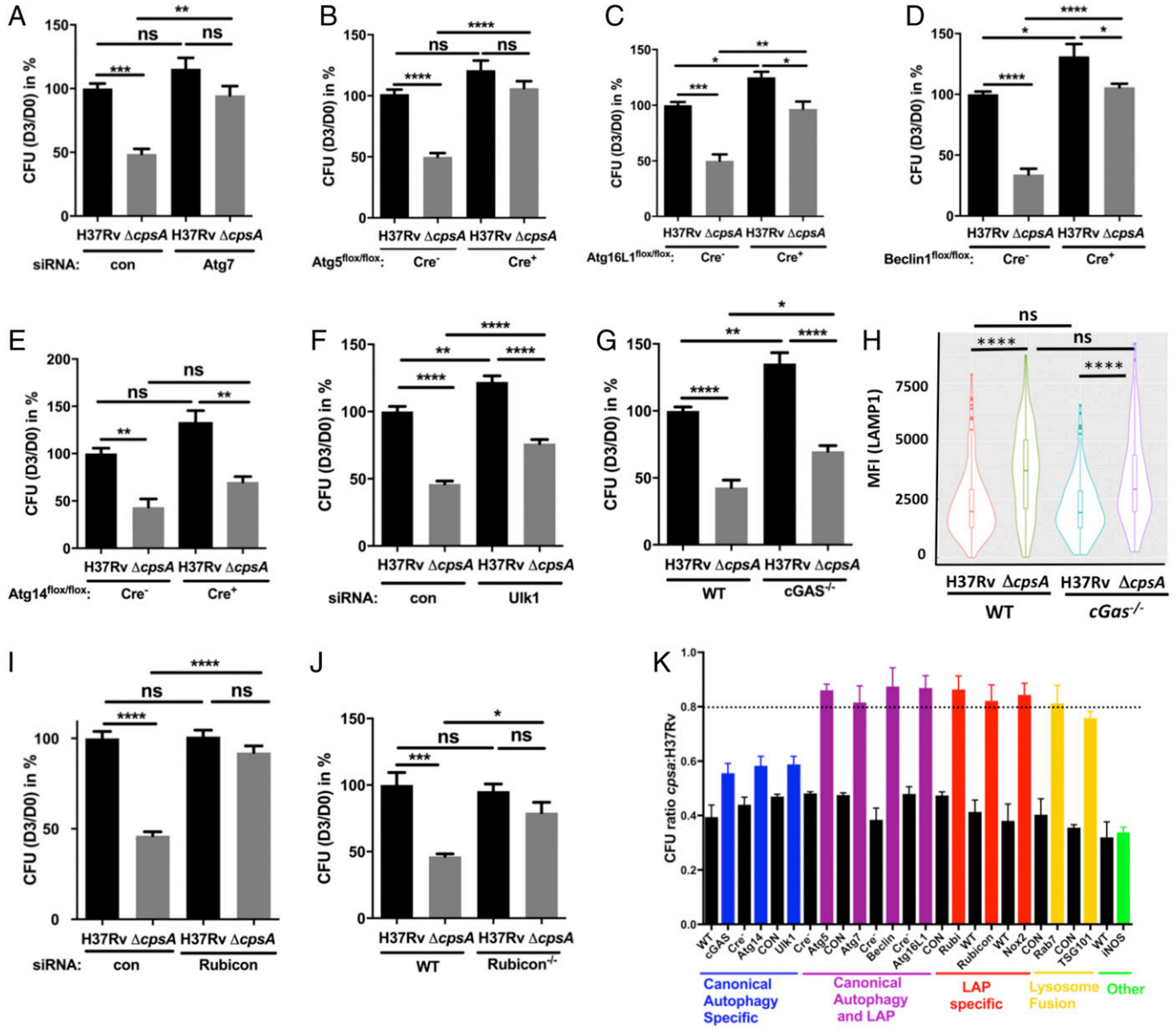

Fig. 3. CpsA-deficient Mtb are cleared by LC3-associated phagocytosis. (*A*, *F*, and *I*) Survival of H37Rv and Δ*cpsA* in BMDMs treated with siRNA control (con) or siRNA targeting Atg7 (*A*), Ulk1 (*F*), or Rubicon (*I*) for 2 d before infection. (*B–E*, *G*, and *J*) Survival of H37Rv and Δ*cpsA* in *Atg5*-KO (*Atg5*$^{flox/flox}$-LysM-Cre^{+}) and control (Atg5$^{flox/flox}$-LysM-Cre^{-}) (*B*), *Atg16L1*-KO (*Atg16L1*$^{flox/flox}$-LysM-Cre^{+}) and control (*Atg16L1*$^{flox/flox}$-LysM-Cre^{-}) (*C*), *Beclin*-KO (*Beclin1*$^{flox/flox}$-LysM-Cre^{+}) and control (*Beclin1*$^{flox/flox}$-LysM-Cre^{-}) (*D*), *Atg14*-KO (*Atg14*$^{flox/flox}$-LysM-Cre^{+}) and control (*Atg14*$^{flox/flox}$-LysM-Cre^{-}) (*E*), WT (C57BL/6) and *Cgas*$^{-/-}$ (*G*), and WT and *Rubicon*$^{-/-}$ BMDMs (*J*). (*H*) Phagosomal LAMP1 quantified 4 hpi in WT or *Cgas*$^{-/-}$ BMDMs from at least 175 bacilli is shown in a violin plot (as described in the legend of Fig. 1). (*K*) The cfu ratios of Δ*cpsA* and H37Rv based on data from *A–G*, *I*, and *J* and Figs. 2 *C* and *D* and 4*A*. Control BMDMs [WT, Cre^{-}, or control-transfected (CON)] are shown in black. Loss-of-function experimental samples are colored according to their biological function as indicated. The dashed line indicates 80% restoration of intracellular growth. In *A–G*, *I*, and *J* the ratios of cfu 3 d after infection relative to day 0 were normalized to the H37Rv control samples. Data show the mean + SEM from one representative experiment with at least three replicates from at least two independent experiments; $*P \le 0.05$; $**P \le 0.01$; $***P \le 0.0005$; $****P \le 0.0001$; ns, not significant; one-way ANOVA with Tukey's multiple comparisons test. Representative data before normalization are shown in Fig. S4.

native promoter (Fig. 7 *A–C*). Because the Δ*cpsA* mutant was attenuated early in infection, it suggested that Mtb requires CpsA to survive the innate immune response, consistent with our findings in macrophages. To further evaluate this, we infected SCID mice, which lack an adaptive immune response. Eight weeks postinfection, all mice infected with a strain producing CpsA died, whereas all Δ*cpsA*-infected mice survived (Fig. 7*D*). Twenty weeks postinfection, we euthanized two of the Δ*cpsA*-infected mice to examine the bacterial burden. Remarkably, we could not recover any bacilli from the lungs. The remaining Δ*cpsA*-infected mice were thriving 32 wk postinfection. These results demonstrate that the innate immune response controls the Δ*cpsA* mutant in vivo, whereas WT Mtb resists the innate immune response, proliferates, and kills the host.

Previous work showed that catalase-deficient Mtb (Δ*katG*) grows equivalently to WT during the first 2 wk of infection in mice, indicating that the bacilli are not experiencing oxidative stress during this time. This observation led McKinney and colleagues to speculate that delivery of NADPH oxidase to Mtb phagosomes is blocked during acute infection (39). Our in vitro data suggested that this might be mediated by CpsA. To determine whether CpsA protects Mtb from NADPH oxidase during acute infection in vivo,

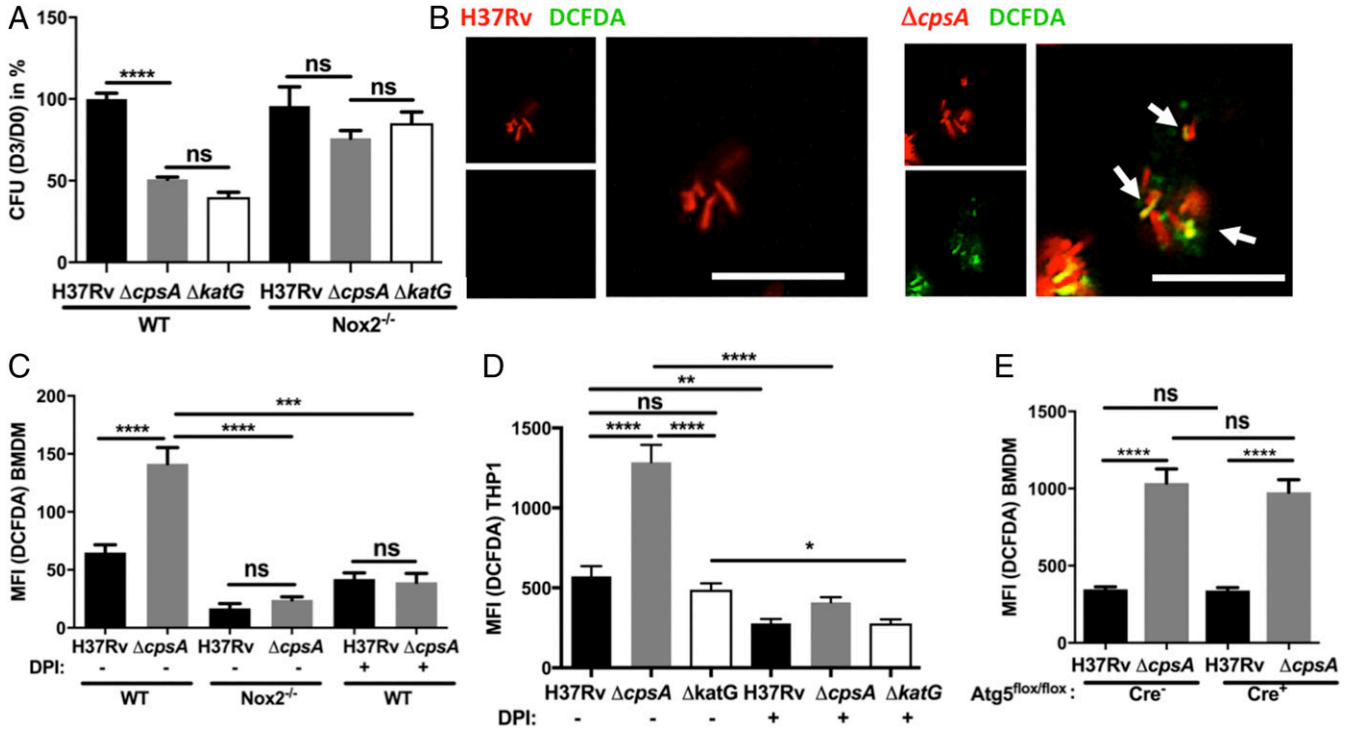

Fig. 4. CpsA blocks NADPH oxidase activity. (*A*) Survival of Mtb H37Rv, Δ*cpsA*, or Δ*katG* in WT and *Nox2*-KO BMDMs. The cfus are shown 3 d after infection relative to day 0 and normalized to WT H37Rv-infected BMDMs. (*B*) Fluorescence microscopy of DsRed-expressing H37Rv or Δ*cpsA* (red) BMDMs at 4 hpi. ROS were visualized with DCFDA (green). Arrows indicate bacilli that colocalize with the DCFDA signal. (Scale bars, 10 μm.) (*C*–*E*) Phagosomal DCFDA was quantified at 4 hpi from WT or *Nox2*-KO BMDMs (*C*), THP-1 cells (*D*), or *Atg5*-KO (*Atg5*$^{flox/flox}$-LysM-Cre^{+}) or control (*Atg5*$^{flox/flox}$-LysM-Cre^{-}) BMDMs (*E*) infected with DsRed-expressing Mtb H37Rv, Δ*cpsA*, or Δ*katG*. In *C* and *D*, control samples were treated with 5 μM DPI during the infection and the DCFDA incubation step as indicated. In *A* and *C*–*E*, data show mean + SEM of one representative experiment from at least two independent experiments in which at least 100 bacilli were analyzed; *$P \leq 0.05$; **$P \leq 0.01$; ***$P \leq 0.0005$; ****$P \leq 0.0001$; ns, not significant; one-way ANOVA with Tukey's multiple comparisons test.

we infected *Nox2*-KO mice with the Δ*cpsA* mutant and compared cfu in the lungs of these mice with that of C57BL/6 mice 17 d postinfection. We found that Δ*cpsA* grew 0.5 log more in the *Nox2*-KO mice than in WT mice (Fig. 7*E*), while *Nox2* did not significantly affect WT Mtb. There was a trend toward increased growth of WT Mtb in mice lacking *Atg5* in the myeloid compartment (*Atg5*$^{flox/flox}$ LysM-Cre^{+}) compared with control animals, while no difference was observed in mice lacking *Atg7* (*Atg7*$^{flox/flox}$ LysM-Cre^{+}), consistent with findings by Kimmey et al. (8). In both *Atg5* and *Atg7* mutants, we observed partial rescue of the Δ*cpsA* mutant compared with Cre^{-} littermate controls (Fig. 7 *F* and *G*). Finally, in keeping with our in vitro data, *Atg14* (*Atg14*$^{flox/flox}$ LysM-Cre^{+}) and *cGAS*-deficient mice failed to rescue the Δ*cpsA* mutant (Fig. 7 *H* and *I*). Overall, our data demonstrate that CpsA protects Mtb from NADPH oxidase and LAP in macrophages and mice.

Discussion

Mtb activates PRRs such as TLR2 and C-type lectin receptors (CLRs) but resists immune control from NADPH oxidase and LAP, which are normally activated by these PRRs. Our findings establish a role for CpsA in evading these antimicrobial pathways. Our results are consistent with previous work showing that NADPH oxidase fails to assemble on the mycobacterial phagosome and that the oxidative burst to Mtb is marginal (39, 43). Previous studies also suggested that Mtb inhibits NADPH oxidase in vivo during acute infection, since catalase-deficient Mtb grow normally during that time (39). Our data demonstrate that CpsA is a significant mediator of Mtb's resistance to NADPH oxidase and LAP in vivo, as the growth of the mutant is improved in mice deficient in *Nox2* or lacking *Atg5* or *Atg7* in hematopoietic cells, all of which are required for LAP. While recent work has called into question the role of autophagy in Mtb pathogenesis (8), our findings suggest that Atg proteins involved in LAP are poised to play a role but are subverted by the pathogen.

NAPDH oxidase and LAP are crucial in the battle of host and pathogen, and our data demonstrate that CpsA plays an important role in Mtb's ability to disarm the innate immune system. The Δ*cpsA* mutant is highly attenuated early during infection before the initiation of an adaptive immune response, and, remarkably, SCID mice do not succumb to infection. Our data highlight that even though Mtb is relatively resistant to ROS by virtue of catalase, NADPH oxidase plays an additional role in bacterial control by activating a potent lysosomal-trafficking pathway. The importance of blocking LAP is demonstrated by other pathogens as well. The growth of *Salmonella typhimurium* is restricted by LAP (40), and *Aspergillus* and *Leishmania* inhibit LAP (44, 45). In addition, a number of pathogens inhibit NADPH oxidase (46–49), although the link to LAP has not been clearly established. Even though Mtb can inhibit NADPH oxidase and LC3-trafficking systems, it must do so imperfectly, as these host mechanisms still play an important role in defense. For example, individuals with chronic granulomatous disease who have mutations in NADPH oxidase have increased susceptibility to mycobacterial diseases (50). We speculate that there may also be rare individuals who are relatively resistant to infection because Mtb cannot disarm their NADPH oxidase and LAP pathway.

Interestingly, the Δ*cpsA* mutant is less attenuated over time in mice (Fig. 7*A*), and it survives similarly to WT Mtb in activated macrophages (Fig. 2 *A* and *B*). These findings suggest that once an adaptive immune response is initiated, different bacterial effectors compensate for the loss of *cpsA* or, alternatively, NADPH oxidase and LAP take on a less important role during chronic infection. We favor the idea that NADPH oxidase and LAP become less important as iNOS and canonical autophagy are

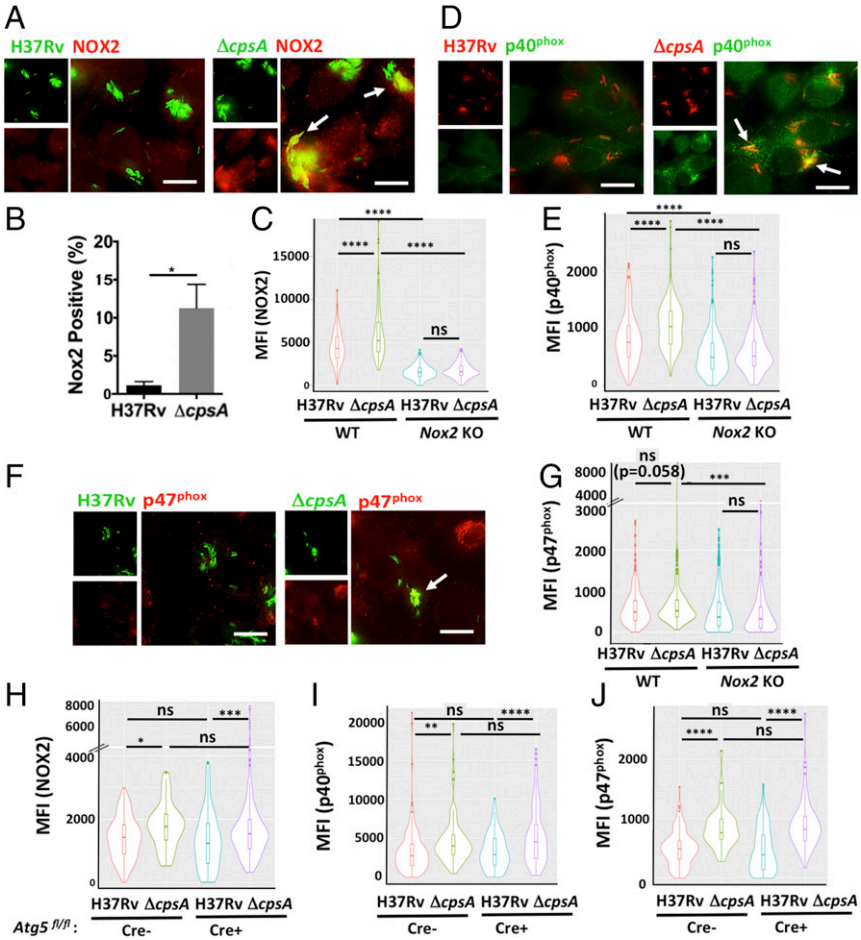

Fig. 5. CpsA inhibits trafficking and assembly of NADPH oxidase. (*A*) IF images of NOX2 (gp91^{phox}) (red) and GFP-expressing H37Rv or Δ*cpsA* (green) WT BMDMs at 4 hpi. (*B*) The percentage of bacteria that colocalized with NOX2 was quantified by a blinded observer from over 400 bacteria. *$P = 0.025$; Student's *t* test. (*C*) Automated image analysis of more than 200 individual bacilli was used to quantify the MFI of NOX2 colocalized with H37Rv and Δ*cpsA* mutant in WT and *Nox2*-KO BMDMs; results are shown as violin plots. (*D*) IF images of p40^{phox} (green) and H37Rv or Δ*cpsA* (red) in WT BMDMs at 4 hpi. (*F*) p47^{phox} (red) and H37Rv or Δ*cpsA* (green) in WT BMDMs at 4 hpi. In *A*, *D*, and *F*, arrows indicate bacilli that colocalize with gp91^{phox}, p40^{phox}, or p47^{phox}. (Scale bars, 10 μm.) (*E* and *G*) Quantification of phagosomal p40^{phox} (*E*) and p47^{phox} (*G*) in WT and *Nox2*-KO BMDMs. (*H–J*) Quantification of phagosomal NOX2/gp91^{phox} (*H*), p40^{phox} (*I*), and p47^{phox} (*J*) in *Atg5*-KO (*Atg5*$^{flox/flox}$-LysM-Cre^{+}) and control (*Atg5*$^{flox/flox}$-LysM-Cre^{-}) cells at 4 hpi with H37Rv or Δ*cpsA*. In *C*, *E*, and *G–J*, data are shown as violin plots (described in the legend of Fig. 1) from a representative experiment from at least two independent experiments. The number of bacilli analyzed per sample was at least 160 in *C*, *E*, and *G* and at least 48 in *H–J*; *$P \leq 0.05$; **$P \leq 0.01$; ***$P \leq 0.0005$; ****$P \leq 0.0001$; ns, not significant; one-way ANOVA with Tukey's multiple comparisons test.

stimulated under the influence of proinflammatory cytokines. At the same time, there would presumably be a corresponding shift in the virulence factors that Mtb needs to persist. Interestingly, two bacterial factors that impair Mtb autophagy in vitro, Eis and PE_PGRS47, do not play a role in acute infection in mice (16, 17). The PE_PGRS47-KO strain is attenuated during chronic infection, perhaps reflecting a switch from LAP to canonical autophagy as a dominant host response in the transition from acute to chronic infection.

CpsA is absent from nonpathogenic mycobacteria, so it appears that duplication of an LCP protein allowed CpsA to acquire an additional role in virulence. The evolution of critical virulence factors from proteins that play a basic role in bacterial physiology in environmental mycobacteria is a recurrent theme in Mtb pathogenesis, perhaps reflecting the lack of horizontal gene transfer. In *Mycobacterium marinum*, the close relative of Mtb, a *cpsA* transposon mutant is also defective in arresting phagosome maturation in macrophages and is attenuated in zebrafish (51). Interestingly, however, in *M. marinum cpsA* seems to have a prominent role in cell-wall biology that is starkly diminished in Mtb. The *M. marinum cpsA* mutant has numerous phenotypes associated with a cell-wall defect, including an in vitro growth defect, altered colony morphology, excess clumpiness, increased susceptibility to certain antibiotics, and enhanced uptake into macrophages (51). The Mtb Δ*cpsA* mutant did not exhibit any of these phenotypes in our studies (Fig. 2 *A* and *B* and Figs. S3*A*, S4 *F–I*, and S7), nor did we find differences in cell-wall extractable lipids or biofilm formation (Figs. S7*D* and S8). Likewise, it was recently reported that the Δ*cpsA* mutant in the CDC1551 strain background did not exhibit significant differences in growth, cording, antibiotic susceptibility, or total lipids, mycolic acids, or cell-wall polysaccharides (21). Thus, CpsA may play a diminished role in cell-wall biogenesis in Mtb compared with *M. marinum*. Another explanation for the differences is that the *M. marinum* mutation is caused by a transposon insertion between the LCP and LytR domains, whereas the Mtb studies used complete deletions. Thus, it is also possible that the prominent cell-wall defects in *M. marinum* are a consequence of an aberrant, truncated CpsA protein.

It remains to be determined how CpsA impairs NADPH oxidase recruitment and LAP. It is possible that it does so as a consequence of its cell-wall function. There is precedence for such a possibility: in *Aspergillus* melanin inhibits recruitment of the p22^{phox} subunit of the NADPH oxidase to germinating conidia,

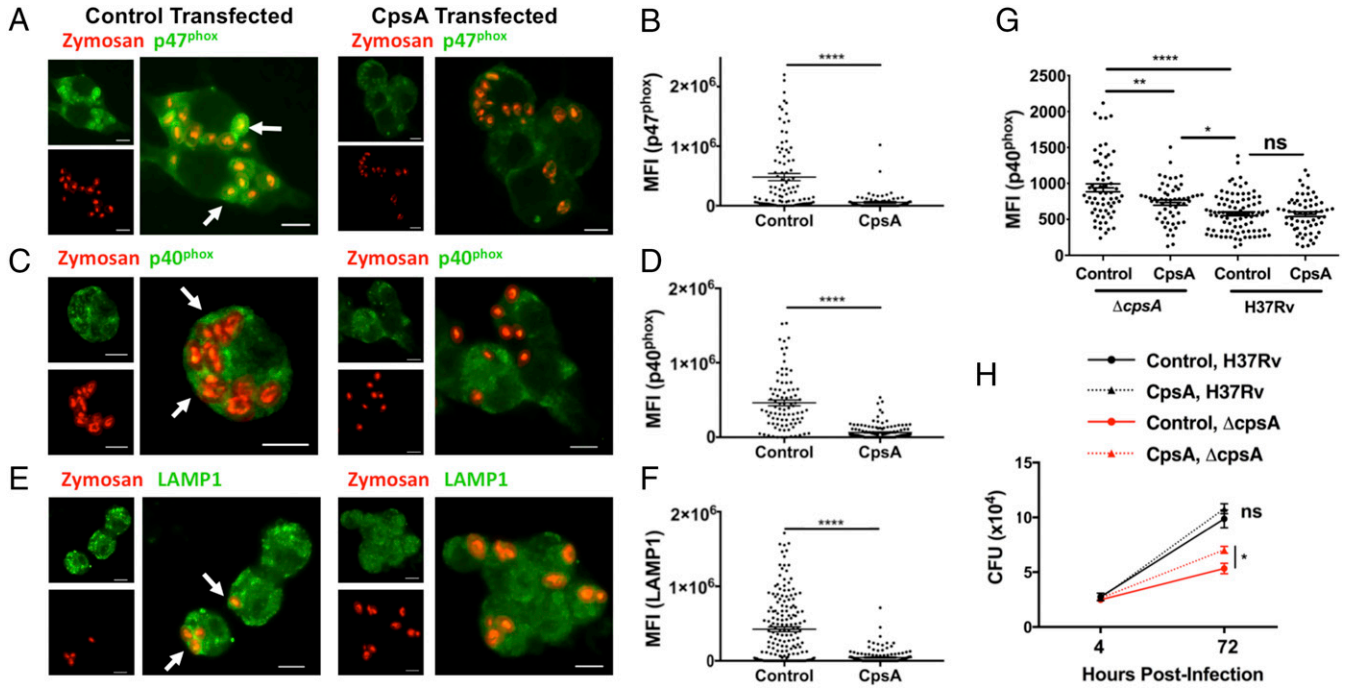

Fig. 6. CpsA is sufficient to inhibit LAP. (*A*, *C*, and *E*) RAW264.7 cells transfected with CpsA or control mRNA were examined by IF microscopy after the addition of zymosan (red) for the localization of p47^{phox} (*A*), p40^{phox} (*C*), and LAMP1 (*E*) (all pseudocolored green). Arrows indicate zymosan particles that colocalize with p47^{phox}, p40^{phox}, or LAMP1. (Scale bars, 10 μm.) (*B*, *D*, and *F*) Quantification of phagosomal p47^{phox} (*B*), p40^{phox} (*D*), and LAMP1 (*F*). (*G*) RAW264.7 cells transfected with CpsA or control mRNA were infected with H37Rv and Δ*cpsA* and were examined by IF microscopy. Phagosomal p40^{phox} was quantified at 3 hpi. (*H*) Growth of H37Rv and Δ*cpsA* in RAW264.7 cells transfected with CpsA or control mRNA. The cfus are shown at the indicated time points. Data show mean ± SEM from one representative experiment from two independent experiments; *$P \leq 0.05$, **$P \leq 0.01$; ****$P \leq 0.0001$; Student's *t* test (*B*, *D*, *F*, and *H*) or ANOVA (*G*).

thereby protecting them from LAP (44). The most straightforward explanation for the macrophage phenotype of the Δ*cpsA* mutant would be that loss of cell-wall integrity results in enhanced PRR signaling, driving LAP. However, our data argue against that possibility. First, the cell wall-associated phenotypes of Δ*cpsA* are subtle, and there were no differences in the proteins shed into culture filtrate by the Δ*cpsA* mutant, arguing against a major disruption to the cell wall. This does not rule out a cell-wall role, but if CpsA inhibits LAP through a cell-wall mechanism, it must carry out an immunologically important but structurally minor modification. Importantly, however, we did not detect any increase in host signaling pathways in response to the Δ*cpsA* mutant to suggest that TLR or CLR signaling were enhanced. In fact, we found the opposite, which may reflect the known ability of NADPH oxidase to negatively regulate NF-κB signaling (52). Thus, CpsA is likely to inhibit LAP downstream of PRRs, raising the possibility that CpsA blocks NADPH oxidase independently of its cell-wall activity. Consistent with this, we found that CpsA dramatically inhibited NADPH oxidase recruitment to zymosan particles, strongly supporting that idea that CpsA has a function independent of the cell wall. In addition, CpsA expression in macrophages partially restored survival of the Δ*cpsA* mutant, arguing that any potential cell-wall defect is not the sole basis of its attenuation.

LCP domain-containing proteins are found in nearly all Gram-positive bacteria, but the paradigm that they play a role in cell-envelope biogenesis is derived from only a few studies. Individual bacterial species can contain up to 11 LCP proteins, and there is at least one example in which an LCP protein serves as a glycosyl transferase that modifies a protein, not PGN (53). Thus, we favor the idea that CpsA has repurposed the LCP domain's transferase activity to target the host. Exactly how CpsA blocks LAP and its relationship to NDP52 and/or TAX1BP1 binding (24) are under investigation.

In conclusion, our studies reveal that Mtb evades LAP, which unexpectedly depends upon the LCP protein, CpsA. Since Mtb strains that induce more ROS or LC3-associated pathways correlate with more favorable treatment outcomes (54, 55), CpsA might be an effective drug target, which could work in concert with host-directed therapies aimed at increasing LC3-trafficking pathways. Moreover, inhibitors that block multiple LCP family members would be particularly attractive therapies, since they would undermine both cell-wall homeostasis and virulence.

Materials and Methods

Bacterial Strains and Growth Conditions. Mtb strain H37Rv was used to generate Δ*cpsA*, Δ*cpsA*::*cpsA*, and Δ*katG*. Mtb strains were grown at 37 °C in 7H9 medium (Middlebrook 7H9 broth; Difco) supplemented with 0.05% Tween 80 (Sigma), BBL Middlebrook OADC Enrichment, and 0.2% glycerol (Sigma). The unmarked Δ*katG* strain was a gift from W. Jacobs, Jr., Albert Einstein College of Medicine, New York. Middlebrook 7H10 or 7H11 agar (BD) was used for growth on solid medium. Δ*cpsA* strain construction and antibiotic selection for plasmids are described in *SI Materials and Methods*. Lysozyme, hydrogen peroxide, nitric oxide, and SDS treatments are described in *SI Materials and Methods*.

Mice. The New York University School of Medicine (NYU SOM) or the Washington University School of Medicine, St. Louis, MO (WUSM) Institutional Animal Care and Use Committee approved all work with mice. C57BL/6, SCID (*Prkdc*^{scid}), and *iNOS* (*Nos2*^{tm1Lau}) mice were obtained from The Jackson Laboratory. *Cgas*$^{-/-}$, *Beclin1*$^{flox/flox}$-*LysM-Cre*, *Atg7*$^{flox/flox}$-*LysM-Cre*, *Atg14*$^{flox/flox}$-*LysM-Cre*, and *Atg16l1*$^{flox/flox}$-*LysM-Cre* mice were generously provided by H. W. Virgin (WUSM). *Rubicon*$^{-/-}$ mice were provided by D. Young (St. Jude Children's Research Hospital, Memphis, TN). *Atg5*$^{flox/flox}$-*LysM-Cre* mice were provided by C. Stallings (WUSM). *Nox2*-KO mice were provided by M. Dinauer (WUSM). LC3-GFP mice were provided by A. Yamamoto (Columbia University, New York) and N. Muzushima (University of Tokyo, Tokyo).

Plasmid Construction. The *cpsA*-complementing plasmid (pKP617) was generated by PCR amplification of the *cpsA* gene along with a 685-bp upstream region as described in *SI Materials and Methods*. For expression in mammalian cells, CpsA-GFP was amplified by PCR and cloned into pDEST47 as described in *SI Materials and Methods*.

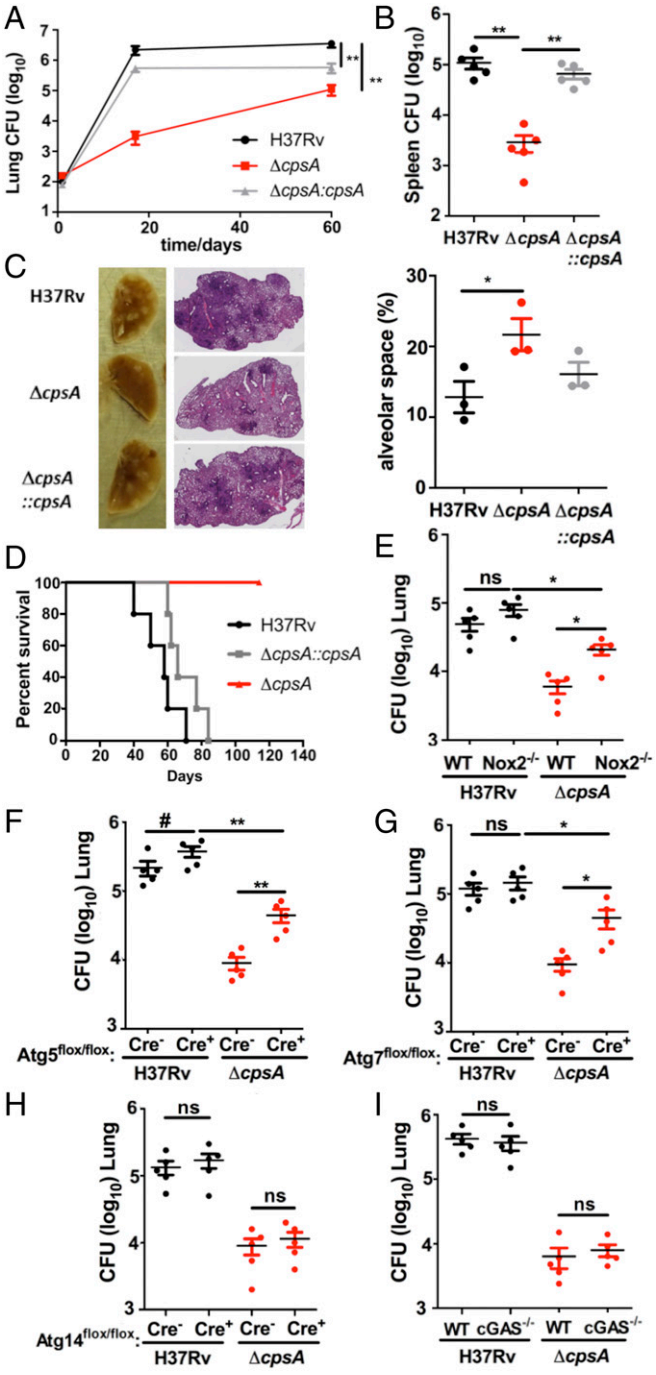

Fig. 7. CpsA is required for innate immune evasion in mice. (*A* and *B*) WT (C57BL/6) mice were infected by aerosol with H37Rv, Δ*cpsA*, or Δ*cpsA::cpsA*. The cfus were enumerated from lungs (*A*) and spleens (*B*) at 60 d postinfection; $n = 5$ mice per group; data show the mean ± SEM; $^{**}P \leq 0.01$; Mann–Whitney test. (*C*) Representative images of the lungs and H&E stains from mice at 60 d postinfection. The alveolar space was calculated from lung sections of three mice using ImageJ; data show mean ± SEM; $^{*}P \leq 0.05$; Student's *t* test. (*D*) Kaplan–Meier survival analysis of SCID mice infected by aerosol with H37Rv, Δ*cpsA*, or Δ*cpsA::cpsA*; $n = 5$ mice per group. The log-rank (Mantel–Cox) test indicated statistical significance between Δ*cpsA* and both H37Rv and Δ*cpsA::cpsA*. ($P \leq 0.0005$). (*E–I*) The cfus were quantified from the lungs of WT and *Nox2*-KO mice (*E*), *Atg5*-KO ($Atg5^{flox/flox}$-LysM-Cre^{+}) mice and $Atg5^{flox/flox}$-LysM-Cre^{-} littermate controls) (*F*), *Atg7*-KO ($Atg7^{flox/flox}$-LysM-Cre^{+}) mice and $Atg7^{flox/flox}$-LysM-Cre^{-} littermate controls (*G*), *Atg14*-KO ($Atg14^{flox/flox}$-LysM-Cre^{+}) mice and $Atg14^{flox/flox}$-LysM-Cre^{-} littermate controls (*H*), and WT and $cGAS^{-/-}$ mice (*I*) infected by aerosol with H37Rv or Δ*cpsA*. Lungs were harvested on day 17 (*E*), 20 (*G* and *I*), 21 (*H*), and 24 (*F*). In *E* and *I*, C57BL/6 (WT) mice were used as controls. $n = 5$ mice per group; data show mean ± SEM; $^{\#}P < 0.10$, $^{*}P \leq 0.05$, $^{**}P \leq 0.01$; ns, not significant; Mann–Whitney test.

Macrophages. Murine hematopoietic stem cells were isolated from the tibia and femurs of 6- to 15-wk-old C57BL/6 mice (unless otherwise noted) as described in *SI Materials and Methods*. THP-1 cells (American Type Culture Collection) and RAW264.7 cells (American Type Culture Collection) were grown as described in *SI Materials and Methods*. RNAi-mediated silencing was performed as described in *SI Materials and Methods*.

Microscopy. Macrophages were infected with GFP- or DsRed-expressing Mtb strains at a multiplicity of infection (MOI) of ∼5. After 4 h, macrophages were washed and fixed with 1% paraformaldehyde/PBS overnight. Immunostaining, ROS visualization, and image acquisition were performed as described in *SI Materials and Methods*.

For the zymosan-trafficking assay, RAW264.7 cells were transfected with CpsA-GFP or CAT-GFP (as control) as described in *SI Materials and Methods*. The transfected macrophages were challenged with Zymosan A Bioparticle Alexa Fluor 594 conjugate (Z23374; Molecular Probes, Life Technologies). Immunostaining, image acquisition, and analysis are described in *SI Materials and Methods*.

Intracellular Bacterial Survival Assays. To assess Mtb survival in vitro, BMDMs from C57BL/6 mice, unless otherwise specified, were seeded 1 d before infection and infected with a single-cell suspension of Mtb at a MOI of ∼3, as previously described (24) and detailed in *SI Materials and Methods*. RAW264.7 cells were used when macrophages were transfected with CpsA as described in *SI Materials and Methods*.

Protein Extracts, Western Blotting, Mass Spectrometry, and RNA-Sequencing. Preparation of protein extracts, Western blotting, mass spectrometry, and RNA-sequencing (RNA-seq) are described in *SI Materials and Methods*.

In Vivo Bacterial Infection. Mice (8–15 wk old) were infected by aerosol with Mtb using the inhalation exposure system from Glas-Col as described in *SI Materials and Methods*. Male and female mice were used except in the case of the *Nox2*-KO mice, for which hemizygous mutant males were compared with WT males. Approximately 100 cfus were administered per animal, except in the case of SCID mice, to which ∼20 cfu were delivered.

Generation of Anti-CpsA Antisera. To generate polyclonal antisera against Mtb CpsA, 250 μg of recombinant CpsA (amino acids 51–512) was produced in *Escherichia coli* and injected into rabbits using TiterMax Gold adjuvant (TiterMax), followed by boosts with incomplete Freund's adjuvant containing 125 μg purified CpsA (Covance).

Glycosyl Composition of Cell Walls (Table S1). Cell walls from Mtb grown to log phase were hydrolyzed with 2 M trifluoroacetic acid, and the derived alditol acetates were subjected to GC/MS as described (21).

Statistical Analysis. The unpaired, two-tailed Student's *t* test, one-way ANOVA with Tukey's multiple comparisons test, or Mann–Whitney test were used to assess the statistical significance of the comparison of experimental groups using GraphPad Prism software (www.graphpad.com). For analysis of Kaplan–Meier curves, the Mantel–Cox (log-rank) survival analysis was used. Violin plots were generated using ggplot2.

ACKNOWLEDGMENTS. We thank M. Dinauer (WUSM), H. W. Virgin (WUSM), D. Young (St. Jude's Children's Research Hospital), N. Mizushima (University of Tokyo), A. Yamamoto (Columbia University), and K. Cadwell (NYU SOM) for their generosity in providing mice; W. Jacobs, Jr. (Albert Einstein College of Medicine) for the Δ*katG* strain; BEI Resources for the anti-KatG antibody; J. Ernst (NYU SOM) for the anti-Ag85 antibody; M. Dinauer, H. W. Virgin, L. D. Sibley (WUSM), A. C. M. Boon (WUSM), and members of the J.A.P. laboratory for useful discussions and helpful comments on the manuscript; Jessica Chapman-Lim and Beatrix Ueberheide (NYU Proteomics Laboratory) for assistance with mass spectrometry; and Eric Tycksen and the Genome Technology Access Center (GTAC) in the Department of Genetics at WUSM for help with genomic analysis and violin plots. The work was supported by funding from the Potts Memorial Foundation (S.K.), Stony Wold-Herbert Fund (S.K.), NIH/NIAID Grant AI119670 (to M.J.), NIH/NIAID Grants AI107774 and AI064282 (to C.M.S.), NIH/NIAID Grant AI130454 (to J.A.P.), and by NYU SOM

and WUSM. The protein mass spectrometry experiments were supported by NIH Shared Instrumentation Grant 1S10OD010582. Development of mice used in this publication was supported by NIH/NIAID Center of Excellence in Translational Research Award Number U19AI109725. The GTAC is partially supported by National Cancer Institute Cancer Center Support Grant P30 CA91842, Institute of Clinical and Translational Sciences/Clinical and Translational Science Award Grant UL1TR000448 from the National Center for Research Resources, and NIH Roadmap for Medical Research.

1. Stanley SA, Cox JS (2013) Host-pathogen interactions during Mycobacterium tuberculosis infections. *Curr Top Microbiol Immunol* 374:211–241.
2. Cemma M, Brumell JH (2012) Interactions of pathogenic bacteria with autophagy systems. *Curr Biol* 22:R540–R545.
3. Huang J, Brumell JH (2014) Bacteria-autophagy interplay: A battle for survival. *Nat Rev Microbiol* 12:101–114.
4. Martinez J, et al. (2015) Molecular characterization of LC3-associated phagocytosis reveals distinct roles for Rubicon, NOX2 and autophagy proteins. *Nat Cell Biol* 17:893–906.
5. Mehta P, Henault J, Kolbeck R, Sanjuan MA (2014) Noncanonical autophagy: One small step for LC3, one giant leap for immunity. *Curr Opin Immunol* 26:69–75.
6. Castillo EF, et al. (2012) Autophagy protects against active tuberculosis by suppressing bacterial burden and inflammation. *Proc Natl Acad Sci USA* 109:E3168–E3176.
7. Gutierrez MG, et al. (2004) Autophagy is a defense mechanism inhibiting BCG and Mycobacterium tuberculosis survival in infected macrophages. *Cell* 119:753–766.
8. Kimmey JM, et al. (2015) Unique role for ATG5 in neutrophil-mediated immunopathology during M. tuberculosis infection. *Nature* 528:565–569.
9. Kumar D, et al. (2010) Genome-wide analysis of the host intracellular network that regulates survival of Mycobacterium tuberculosis. *Cell* 140:731–743.
10. Manzanillo PS, et al. (2013) The ubiquitin ligase parkin mediates resistance to intracellular pathogens. *Nature* 501:512–516.
11. Sakowski ET, et al. (2015) Ubiquilin 1 promotes IFN-γ-induced xenophagy of Mycobacterium tuberculosis. *PLoS Pathog* 11:e1005076.
12. Watson RO, et al. (2015) The cytosolic sensor cGAS detects Mycobacterium tuberculosis DNA to induce type I interferons and activate autophagy. *Cell Host Microbe* 17:811–819.
13. Watson RO, Manzanillo PS, Cox JS (2012) Extracellular M. tuberculosis DNA targets bacteria for autophagy by activating the host DNA-sensing pathway. *Cell* 150:803–815.
14. Ouimet M, et al. (2016) Mycobacterium tuberculosis induces the miR-33 locus to reprogram autophagy and host lipid metabolism. *Nat Immunol* 17:677–686.
15. Romagnoli A, et al. (2012) ESX-1 dependent impairment of autophagic flux by Mycobacterium tuberculosis in human dendritic cells. *Autophagy* 8:1357–1370.
16. Saini NK, et al. (2016) Suppression of autophagy and antigen presentation by Mycobacterium tuberculosis PE_PGRS47. *Nat Microbiol* 1:16133.
17. Shin DM, et al. (2010) Mycobacterium tuberculosis eis regulates autophagy, inflammation, and cell death through redox-dependent signaling. *PLoS Pathog* 6:e1001230.
18. Chan YG, Kim HK, Schneewind O, Missiakas D (2014) The capsular polysaccharide of Staphylococcus aureus is attached to peptidoglycan by the LytR-CpsA-Psr (LCP) family of enzymes. *J Biol Chem* 289:15680–15690.
19. Eberhardt A, et al. (2012) Attachment of capsular polysaccharide to the cell wall in Streptococcus pneumoniae. *Microb Drug Resist* 18:240–255.
20. Kawai Y, et al. (2011) A widespread family of bacterial cell wall assembly proteins. *EMBO J* 30:4931–4941.
21. Grzegorzewicz AE, et al. (2016) Assembling of the Mycobacterium tuberculosis cell wall core. *J Biol Chem* 291:18867–18879.
22. Harrison J, et al. (2016) Lcp1 is a phosphotransferase responsible for ligating arabinogalactan to peptidoglycan in Mycobacterium tuberculosis. *MBio* 7:e00972-16.
23. McGuire AM, et al. (2012) Comparative analysis of Mycobacterium and related actinomycetes yields insight into the evolution of Mycobacterium tuberculosis pathogenesis. *BMC Genomics* 13:120.
24. Mehra A, et al. (2013) Mycobacterium tuberculosis type VII secreted effector EsxH targets host ESCRT to impair trafficking. *PLoS Pathog* 9:e1003734.
25. de Souza GA, Leversen NA, Målen H, Wiker HG (2011) Bacterial proteins with cleaved or uncleaved signal peptides of the general secretory pathway. *J Proteomics* 75:502–510.
26. de Souza GA, et al. (2008) High accuracy mass spectrometry analysis as a tool to verify and improve gene annotation using Mycobacterium tuberculosis as an example. *BMC Genomics* 9:316.
27. Målen H, Berven FS, Fladmark KE, Wiker HG (2007) Comprehensive analysis of exported proteins from Mycobacterium tuberculosis H37Rv. *Proteomics* 7:1702–1718.
28. Tumbarello DA, et al. (2015) The autophagy receptor TAX1BP1 and the molecular motor myosin VI are required for clearance of Salmonella Typhimurium by autophagy. *PLoS Pathog* 11:e1005174.
29. von Muhlinen N, Thurston T, Ryzhakov G, Bloor S, Randow F (2010) NDP52, a novel autophagy receptor for ubiquitin-decorated cytosolic bacteria. *Autophagy* 6:288–289.
30. Harris J, et al. (2007) T helper 2 cytokines inhibit autophagic control of intracellular Mycobacterium tuberculosis. *Immunity* 27:505–517.
31. Matsuzawa T, et al. (2012) IFN-γ elicits macrophage autophagy via the p38 MAPK signaling pathway. *J Immunol* 189:813–818.
32. Philips JA, Porto MC, Wang H, Rubin EJ, Perrimon N (2008) ESCRT factors restrict mycobacterial growth. *Proc Natl Acad Sci USA* 105:3070–3075.
33. Portal-Celhay C, et al. (2016) Mycobacterium tuberculosis EsxH inhibits ESCRT-dependent CD4(+) T-cell activation. *Nat Microbiol* 2:16232.
34. Collins AC, et al. (2015) Cyclic GMP-AMP synthase is an innate immune DNA sensor for Mycobacterium tuberculosis. *Cell Host Microbe* 17:820–828.
35. Manzanillo PS, Shiloh MU, Portnoy DA, Cox JS (2012) Mycobacterium tuberculosis activates the DNA-dependent cytosolic surveillance pathway within macrophages. *Cell Host Microbe* 11:469–480.
36. Wassermann R, et al. (2015) Mycobacterium tuberculosis differentially activates cGAS- and inflammasome-dependent intracellular immune responses through ESX-1. *Cell Host Microbe* 17:799–810.
37. Matsunaga K, et al. (2009) Two Beclin 1-binding proteins, Atg14L and Rubicon, reciprocally regulate autophagy at different stages. *Nat Cell Biol* 11:385–396.
38. Yang CS, et al. (2012) Autophagy protein Rubicon mediates phagocytic NADPH oxidase activation in response to microbial infection or TLR stimulation. *Cell Host Microbe* 11:264–276.
39. Ng VH, Cox JS, Sousa AO, MacMicking JD, McKinney JD (2004) Role of KatG catalase-peroxidase in mycobacterial pathogenesis: Countering the phagocyte oxidative burst. *Mol Microbiol* 52:1291–1302.
40. Huang J, et al. (2009) Activation of antibacterial autophagy by NADPH oxidases. *Proc Natl Acad Sci USA* 106:6226–6231.
41. Casbon AJ, Allen LA, Dunn KW, Dinauer MC (2009) Macrophage NADPH oxidase flavocytochrome B localizes to the plasma membrane and Rab11-positive recycling endosomes. *J Immunol* 182:2325–2339.
42. Nunes P, Demaurex N, Dinauer MC (2013) Regulation of the NADPH oxidase and associated ion fluxes during phagocytosis. *Traffic* 14:1118–1131.
43. Sun J, et al. (2013) Mycobacterium tuberculosis nucleoside diphosphate kinase inactivates small GTPases leading to evasion of innate immunity. *PLoS Pathog* 9:e1003499.
44. Akoumianaki T, et al. (2016) Aspergillus cell wall melanin blocks LC3-associated phagocytosis to promote pathogenicity. *Cell Host Microbe* 19:79–90.
45. Matte C, et al. (2016) Leishmania major promastigotes evade LC3-associated phagocytosis through the action of GP63. *PLoS Pathog* 12:e1005690.
46. Keith KE, Hynes DW, Sholdice JE, Valvano MA (2009) Delayed association of the NADPH oxidase complex with macrophage vacuoles containing the opportunistic pathogen Burkholderia cenocepacia. *Microbiology* 155:1004–1015.
47. Lam GY, et al. (2011) Listeriolysin O suppresses phospholipase C-mediated activation of the microbicidal NADPH oxidase to promote Listeria monocytogenes infection. *Cell Host Microbe* 10:627–634.
48. McCaffrey RL, et al. (2010) Multiple mechanisms of NADPH oxidase inhibition by type A and type B Francisella tularensis. *J Leukoc Biol* 88:791–805.
49. Siemsen DW, Kirpotina LN, Jutila MA, Quinn MT (2009) Inhibition of the human neutrophil NADPH oxidase by Coxiella burnetii. *Microbes Infect* 11:671–679.
50. Deffert C, Cachat J, Krause KH (2014) Phagocyte NADPH oxidase, chronic granulomatous disease and mycobacterial infections. *Cell Microbiol* 16:1168–1178.
51. Wang Q, et al. (2015) CpsA, a LytR-CpsA-Psr family protein in Mycobacterium marinum, is required for cell wall integrity and virulence. *Infect Immun* 83:2844–2854.
52. Segal BH, Grimm MJ, Khan AN, Han W, Blackwell TS (2012) Regulation of innate immunity by NADPH oxidase. *Free Radic Biol Med* 53:72–80.
53. Wu C, et al. (2014) Lethality of sortase depletion in Actinomyces oris caused by excessive membrane accumulation of a surface glycoprotein. *Mol Microbiol* 94:1227–1241.
54. Li F, Gao B, Xu W, Chen L, Xiong S (2016) The defect in autophagy induction by clinical isolates of Mycobacterium tuberculosis is correlated with poor tuberculosis outcomes. *PLoS One* 11:e0147810.
55. Romero MM, et al. (2014) Outbreaks of Mycobacterium tuberculosis MDR strains differentially induce neutrophil respiratory burst involving lipid rafts, p38 MAPK and Syk. *BMC Infect Dis* 14:262.
56. Murphy KC, Papavinasasundaram K, Sassetti CM (2015) Mycobacterial recombineering. *Methods Mol Biol* 1285:177–199.
57. van Kessel JC, Hatfull GF (2007) Recombineering in Mycobacterium tuberculosis. *Nat Methods* 4:147–152.
58. Banaiee N, Kincaid EZ, Buchwald U, Jacobs WR, Jr, Ernst JD (2006) Potent inhibition of macrophage responses to IFN-gamma by live virulent Mycobacterium tuberculosis is independent of mature mycobacterial lipoproteins but dependent on TLR2. *J Immunol* 176:3019–3027.
59. Tufariello JM, et al. (2016) Separable roles for Mycobacterium tuberculosis ESX-3 effectors in iron acquisition and virulence. *Proc Natl Acad Sci USA* 113:E348–E357.
60. Cotto-Rios XM, Békés M, Chapman J, Ueberheide B, Huang TT (2012) Deubiquitinases as a signaling target of oxidative stress. *Cell Rep* 2:1475–1484.
61. Cox J, et al. (2014) Accurate proteome-wide label-free quantification by delayed normalization and maximal peptide ratio extraction, termed MaxLFQ. *Mol Cell Proteomics* 105:2513–2526.
62. Rengarajan J, et al. (2008) Mycobacterium tuberculosis Rv2224c modulates innate immune responses. *Proc Natl Acad Sci USA* 105:264–269.
63. Wolf AJ, et al. (2007) Mycobacterium tuberculosis infects dendritic cells with high frequency and impairs their function in vivo. *J Immunol* 179:2509–2519.
64. Vandal OH, et al. (2009) Acid-susceptible mutants of Mycobacterium tuberculosis share hypersusceptibility to cell wall and oxidative stress and to the host environment. *J Bacteriol* 191:625–631.
65. Ojha A, et al. (2005) GroEL1: A dedicated chaperone involved in mycolic acid biosynthesis during biofilm formation in mycobacteria. *Cell* 123:861–873.
66. Flentie KN, Stallings CL, Turk J, Minnaard AJ, Hsu FF (2016) Characterization of phthiocerol and phthiodiolone dimycocerosate esters of M. tuberculosis by multiple-stage linear ion-trap MS. *J Lipid Res* 57:142–155.
67. Jain M, et al. (2007) Lipidomics reveals control of Mycobacterium tuberculosis virulence lipids via metabolic coupling. *Proc Natl Acad Sci USA* 104:5133–5138.